Solid State Sciences 17 (2013) 97–101

Contents lists available at SciVerse ScienceDirect

Solid State Sciences

journal homepage: www.elsevier.com/locate/ssscie

Magnetic characteristics of nanocrystalline GaMnN films deposited by reactive sputtering

D.M.G. Leite [a,*], A.L.J. Pereira [a], W.A. Iwamoto [b], P.G. Pagliuso [b], P.N. Lisboa-Filho [a], J.H.D. da Silva [a]

[a] Advanced Materials Group, UNESP – Univ Estadual Paulista, Bauru 17033-360, SP, Brazil
[b] Instituto de Física "Gleb Wataghin", Unicamp, Campinas 13083-970, SP, Brazil

ARTICLE INFO

Article history:
Received 16 April 2012
Received in revised form
14 November 2012
Accepted 25 November 2012
Available online 4 December 2012

Keywords:
Sputtering
GaMnN
Nanocrystalline material
Diluted magnetic semiconductor
Magnetic properties

ABSTRACT

The magnetic characteristics of $Ga_{1-x}Mn_xN$ nanocrystalline films ($x = 0.08$ and $x = 0.18$), grown by reactive sputtering onto amorphous silica substrates (a-SiO_2), are shown. Further than the dominant paramagnetic-like behaviour, both field- and temperature-dependent magnetization curves presented some particular features indicating the presence of secondary magnetic phases. A simple and qualitative analysis based on the Brillouin function assisted the interpretation of these secondary magnetic contributions, which were tentatively attributed to antiferromagnetic and ferromagnetic phases.

1. Introduction

Diluted magnetic semiconductors (DMS) have attracted the attention of several research groups due to their potential for fabrication of functional spintronic devices [1–3]. In particular, $Ga_{1-x}Mn_xN$ is expected – once doped with a sufficient amount of free or weakly localized holes – to show ferromagnetism at room temperature, a critical requirement for practical applications [1–3]. To date, numerous experiments have demonstrated that $Ga_{1-x}Mn_xN$ systems can show ferromagnetism (FM) [4,5], paramagnetism (PM) [6,7], antiferromagnetism (AFM) [8,9] and superparamagnetism (SPM) [10], as a function mainly of the Mn concentration and the microstructure of the sublattice (GaN).

In selected monocrystalline GaMnN samples, where the incorporated Mn is believed to be diluted, either pure paramagnetism [6,7] or room temperature ferromagnetism [4,5] can be found. In this case, the Mn concentration plays a major role: for samples containing up to 1% of diluted Mn ($x = 0.01$), only paramagnetic phase is detected for temperatures from 1.8 to 300 K [6,7], while for Mn concentrations above 3% ($x = 0.03$), a ferromagnetic phase is reported [4] at up to 940 K [5]. However, no consensus has yet been reached about the microscopic mechanisms that give rise to the ferromagnetic phase in monocrystalline GaMnN. Two main approaches have been considered in the literature: the direct double exchange mechanism [11,12] and the carrier mediated Zener model [1,2].

The discussion becomes more complicated when considering nanocrystalline GaMnN systems. In these cases, the presence of a significant portion of disorder – mainly represented by the presence of grain boundaries – gives rise to different geometric and chemical environments for the Mn sites, beyond those expected in a well-organized monocrystalline GaN matrix. This complex situation leads to new possibilities with respect to the magnetic interaction between the Mn ions, even if they are present in a diluted regime. In fact, antiferromagnetism [8,9] and superparamagnetism [10] are commonly reported for nanocrystalline $Ga_{1-x}Mn_xN$ with a variety of Mn concentrations up to 18% ($x = 0.18$). The antiferromagnetism is especially attributed to the presence of a significant portion of Mn^{2+} (d^5) instead of the expected Mn^{3+} (d^4). Furthermore, it is also reasonable to consider the possibility of coexisting magnetic phases in nanocrystalline GaMnN systems. In this case, the results from superconductor quantum interference device (SQUID) magnetometry become quite difficult to interpret, which leads, in most cases, to incomplete or even incorrect conclusions about the real magnetic phases present in this type of material.

* Corresponding author. Departamento de Física, Univ. Estadual Paulista – UNESP, Av. Eng. Edmundo C. Coube, 14-01, CEP 17033-360 Bauru, SP, Brazil. Tel.: +55 (14) 3103 6178; fax: +55 (14) 3103 6084.
E-mail address: dmgleite@fc.unesp.br (D.M.G. Leite).

1293-2558/$ – see front matter © 2012 Elsevier Masson SAS. All rights reserved.
http://dx.doi.org/10.1016/j.solidstatesciences.2012.11.020

In this work, we report a systematic magnetic characterization and analysis of $Ga_{1-x}Mn_xN$ nanocrystalline films ($x = 0.08$ and $x = 0.18$) grown by reactive sputtering onto amorphous silica substrates (a-SiO_2) [13–17]. A simple and qualitative analysis based on the Brillouin function indicate the presence of secondary magnetic contributions tentatively attributed to antiferromagnetic and ferromagnetic phases further than the dominant paramagnetic contribution from non-interacting Mn ions.

2. Experimental details

$Ga_{1-x}Mn_xN$ nanocrystalline films ($x = 0.08$ and 0.18) were grown by reactive sputtering onto amorphous silica (a-SiO_2) at relatively low substrate temperature ($T_S \sim 200$ °C) [13–17]. Only α-GaN (wurtzite) phase could be identified by X-ray diffraction (XRD). High-resolution transmission electron microscopy (HRTEM) and electron diffraction measurements showed that the films treated here are composed of a thin intermediate layer of non-oriented nanocrystals (diameter ~5 nm) and a posterior columnar structure (diameter ~30 nm) that is highly oriented with <0001> direction perpendicular to the film surface [17]. The thickness of the intermediate layer was around 50 nm for $x = 0.08$ and around 65 nm for $x = 0.18$ sample – the total film thicknesses were 900 nm and 640 nm, respectively. Despite the nanostructure of these films, Energy Filtered TEM measurements performed on $x = 0.18$ sample showed no evidence of Mn segregation up to the achieved resolution (5 nm) [17]. It is important to mention that the samples were not intentionally codoped and all the extrinsic carriers probably present should be related to: (i) Mn incorporation in different charge states and (ii) all the possible defects such as vacancies and crystallites surface states.

For the magnetic characterization, selected samples were cut in approximately 5 × 10 mm geometry. In order to avoid any kind of magnetic contamination, special care was taken with the sample manipulation including the use of plastic tweezers only, the use of previously tested diamagnetic plastic tubes to contain the samples, and systematic tests with pure substrates. These precautions are strictly necessary due to the very low magnetic moments of the samples and the high sensitivity of the SQUID magnetometer, as pointed out by other groups [18].

The magnetic characterization was performed in a SQUID magnetometer using field-dependent magnetization loops with applied magnetic field from −50 to 50 kOe taken at temperatures from 2 to 300 K; and temperature-dependent magnetization curves using zero field cooled (ZFC) and field cooled (FC) loops under applied magnetic field from 0.1 to 10 kOe. All magnetic measurements shown here were performed in the DC configuration with an applied field parallel to the sample surface (in-plane field). Each magnetization point was obtained as the arithmetic average of two sample excursions through the SQUID coils, with each excursion 12 cm long and divided into 25 points.

3. Results

Fig. 1(a) shows the in-plane total magnetization curves for $x = 0.08$ and $x = 0.18$ $Ga_{1-x}Mn_xN$ samples taken at 2 and 300 K. The a-SiO_2 substrate magnetization curve taken at 2 K was added for comparison: the same response is obtained at 300 K, which indicates pure diamagnetic behaviour. In Fig. 1(a), the total magnetization has been simply determined using the total mass (film + substrate) of each sample. In Fig. 1(b), the substrate diamagnetism has been appropriately subtracted from the GaMnN samples and the magnetization was now determined by the film volume of the $x = 0.08$ and $x = 0.18$ samples (4.94×10^{-5} cm^3 and 1.66×10^{-5} cm^3, respectively).

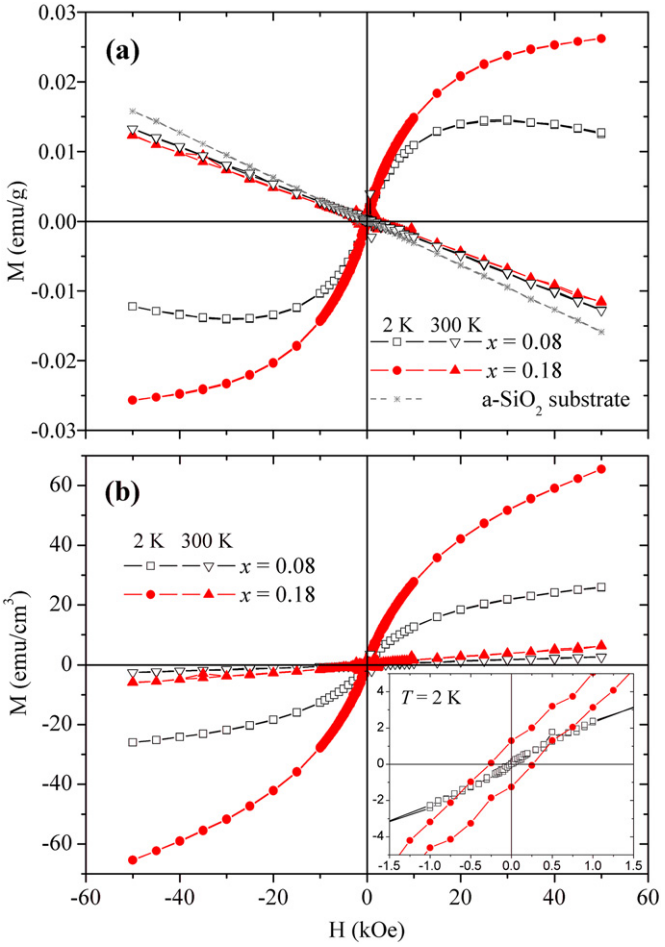

Fig. 1. (a) Total magnetization curves for $x = 0.08$ and $x = 0.18$ $Ga_{1-x}Mn_xN$ samples taken at 2 K and 300 K. The magnetization of a pure a-SiO_2 substrate taken at 2 K was added for comparison. The total mass of each sample was used to determine the total magnetization in emu/g. (b) Corrected magnetization curves obtained by subtracting the substrate diamagnetism and using the respective film volume to determine the magnetization in emu/cm^3.

After the correction, the magnetization curves in Fig. 1(b) and in all of the following graphs can be, in a first approximation, directly related to the presence of Mn ions in the samples. This is due to the fact that our pure GaN sample ($x = 0.00$) been purely diamagnetic with practically the same susceptibility as the pure a-SiO_2 substrate, furthermore, no magnetic anisotropy was observed by performing in-plane and out-of-plane measurements.

Despite of the fact that *M vs H* curves show typical paramagnetic characteristics: smooth S-shape at low temperatures ($T < 50$ K) and a linear shape with weak positive susceptibility at higher temperatures ($T > 100$ K); two remarks should be emphasised: (i) the presence of a weak hysteresis loop at $T = 2$ K for the sample with highest Mn content ($x = 0.18$) shown in the inset of Fig. 1(b); and (ii) a quasi-linear increase of the magnetization for $H > 20$ kOe for $T = 2$ K for both samples (Fig. 1(b)). Both features indicate that secondary magnetic phases, further than an ordinary paramagnetic phase, are contributing to the total magnetization of the studied samples. In fact, the tentative of describing our experimental *M vs H* curves at $T < 50$ K with a unique Brillouin function (Equation (1)) just fails.

For this reason, and in order to get a better but still qualitative insight into the possible magnetic phases present, the following procedure, based on the use of multiple Brillouin functions and supported by recent literature [2,8,9], is adopted here. In the

proposed approach, the experimental magnetization is approximated by a theoretical magnetization M which consists on the sum of up to three components ($M = M_1 + M_2 + M_3$), each of them represented by a Brillouin function ($M_i = x_i^{\text{eff}} N_0 g J_i \mu_B B_{J_i}(y)$) applied to a magnetic domain with total magnetic momentum J_i and effective concentration x_i^{eff}. Here N_0 is the total number of cation (Ga + Mn) sites, μ_B and k_B are the Bohr magneton and the Boltzmann constant respectively, and g is the Landé factor.

$$B_J(y) = \frac{2J+1}{2J}\coth\left(\frac{2J+1}{2J}y\right) - \frac{1}{2J}\coth\left(\frac{1}{2J}y\right) \quad (1)$$

$$y = \frac{gJ\mu_B H}{k_B T}$$

In the present work, the paramagnetic contribution from isolated Mn ions is approximated by the first magnetic contribution (M_1) applied to $J_1 = 2$ and $g = 2$. The second contribution (M_2) is a low magnetic moment component, which is approximated by a Brillouin function applied to a very small magnetic moment ($J_2 \sim 0.1$ and $g = 2$). The third magnetic contribution (M_3) is a high magnetic moment contribution, which is approximated here as the Brillouin function applied to high magnetic moments ($J_3 \sim 20$ with $g = 2$). The x_i^{eff} values were computationally adjusted to get the best fit to each M *vs* H data.

Representative experimental M *vs* H curves (open circles) from $x = 0.08$ and 0.18 samples are shown in Fig. 2 with the respective best fit (red solid line in the web version) composed by a sum of different Brillouin-based contributions (M_1, M_2 and M_3). It is important to mention that all three contributions were necessary to properly describe the magnetization curves taken at $T < 10$ K. However, only the first and third contributions ($x_2^{\text{eff}} = 0$) were needed to describe the curves taken at temperatures between 10 and 50 K. For temperatures above 100 K, only the first contribution has been necessary ($x_2^{\text{eff}} = 0$ and $x_3^{\text{eff}} = 0$).

The calculation of the temperature-dependent Brillouin curves in 2–300 K range was also possible by linearly interpolating the adjusted x_i^{eff} values for each sample. These calculated curves were then compared to the respective ZFC–FC experimental curves shown in Fig. 3. Despite the presence of small shoulders due to the abrupt variation of the interpolated x_i^{eff}, the agreement between the calculated curves with the experimental data is evident in Fig. 3. This is a good indication that these three magnetic contributions have been properly chosen to approximate the magnetic response of our $Ga_{1-x}Mn_xN$ nanocrystalline samples.

4. Discussion

Both field- and temperature-dependent magnetization data from the sputtered GaMnN samples (Figs. 2 and 3) show typical paramagnetic-like characteristics. However, the possible presence of secondary magnetic contribution is denounced by two main features: (i) the presence of a weak M *vs* H hysteresis loop at $T = 2$ K for $x = 0.18$ sample (inset of Fig. 1(b)); and (ii) the absence of

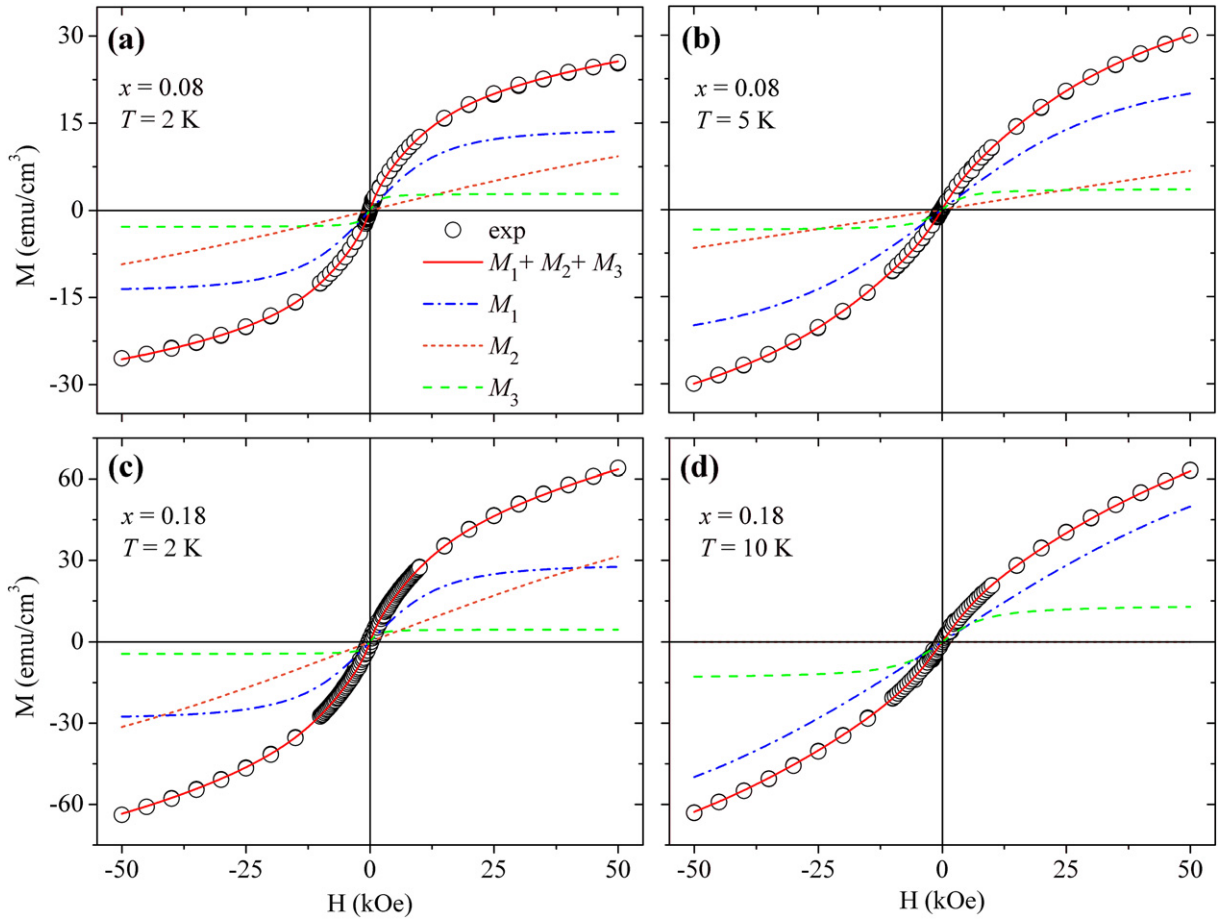

Fig. 2. Experimental magnetization curves (open circles) for $x = 0.08$ taken at (a) 2 K and (b) 5 K, and for $x = 0.18$ taken at (c) 2 K and (d) 10 K. The red solid lines are the best fits to the experimental data using Brillouin functions. The contributing curves (M_1: blue dash-dotted lines, M_2: orange dotted lines, M_3: green dashed lines) were also plotted in each graph. (For interpretation of the references to colour in this figure legend, the reader is referred to the web version of this article.)

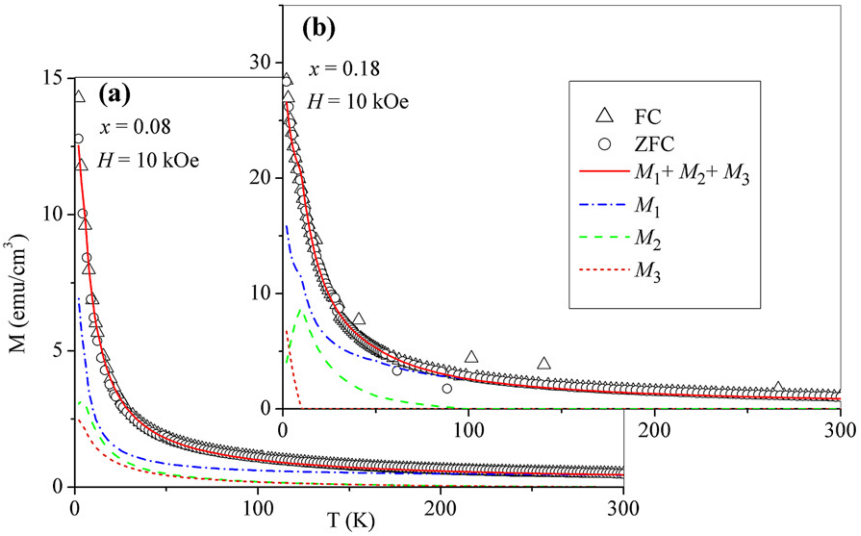

Fig. 3. Experimental temperature-dependent magnetization data for (a) $x = 0.08$ and (b) $x = 0.18$ samples taken with applied field of 10 kOe (open symbols). The red solid lines represent the calculated M *vs* T curves from the sum of each Brillouin contribution (M_1: blue dash-dotted lines, M_2: orange dotted lines, M_3: green dashed lines). (For interpretation of the references to colour in this figure legend, the reader is referred to the web version of this article.)

saturation at $T = 2$ K for both samples (Fig. 1(b)). The presence of one or more secondary contributions is corroborated by two other facts: (iii) the impossibility of describing the M *vs* H data taken at $T = 2$ K by a unique Brillouin function (tried with a variety set of parameters); and (iv) the impossibility of describing the M *vs* T data (Fig. 3) by a unique Brillouin function (tried with a variety set of parameters) nor even by a unique Curie–Weiss law.

Even though the use of multiple Brillouin functions, strictly speaking, can lead to multiple sets of parameters, the qualitative information given by the different Brillouin-like contributions, as described in the previous section, can be useful for understanding the possible magnetic entities behind the overall magnetization response of the GaMnN samples prepared by sputtering.

In fact, the first magnetic contribution (M_1), described here by the Brillouin function with $J_1 = 2$, could be associated with the paramagnetic response of non-interacting Mn^{3+} ions ($S = 2$), which are diluted in the GaN lattice with quenched orbital momentum ($L = 0$ and $g = 2$). However, the use of $g = 2$ is an approximation itself since a non-quenched orbital momentum L is expected for some special directions in the hexagonal symmetry.

Still concerning the first contribution, it is worth to mention that a good agreement with the experimental data can also be achieved by using $J_1 = 5/2$ instead of $J_1 = 2$. Thus, from the Brillouin fittings, it is not possible to distinguish the contribution of paramagnetic Mn^{2+} ($S = 5/2$) or Mn^{3+} ($S = 2$) centres that are probably found in the studied films mainly due to their nanocrystalline nature, which provides different environments for the Mn sites. However, the presence of Mn^{3+} ions was previously confirmed by the optical characterization [15] of these GaMnN films, making more probable that the non-interacting Mn^{3+} ions are dominating the paramagnetic response here approximated by M_1.

The second contribution described by M_2 is treated here as the responsible for increasing the magnetization in a quasi-linear fashion after the saturation of the paramagnetic contribution (M_1) in the M *vs* H experiments at low temperatures ($H > 20$ kOe at $T = 2$ K). The characteristics of this second contribution can be achieved by a Brillouin function applied to a very small magnetic moment ($J_2 \sim 0.1$) or, alternatively, by a Brillouin function with expected J values for Mn ions ($J_2 = 5/2$ or $J_2 = 2$) but introducing the effective temperature $T^{eff} = T + T^0$. Here T is the measured temperature, and $T^0 > 0$ is the displacement temperature, assumed to reflect the presence of antiferromagnetic interaction between Mn ions [2,8,9].

However, before attempting to correlate the M_2 contribution to a possible presence of an AFM phase, it is worth mentioning that the characteristics of the M_2 contribution (quasi-linear M *vs* H curve at $T \sim 2$ K) have also been reported [6] for $Ga_{1-x}Mn_xN$ single crystals ($x \sim 0.01$) when the applied field is parallel to the wurtzite c-axis ($H//c$). According to W. Stefanowicz et al. [6], the anisotropic tetrahedral crystal field is responsible for the non-quenched orbital momentum ($L \neq 0$) of Mn^{3+} ions in $H//c$ geometry. This leads to a particular magnetization behaviour at $T \sim 2$ K that is very similar to that expected from a low-spin paramagnetism ($J_2 \sim 0.1$ as used in M_2). Based on the above findings and on the nanocrystalline structure of our films [17], the M_2 contribution still could be assumed to represent the response of non-interacting Mn ions. However, unlike those ions contributing to M_1, these are incorporated into crystallites that have their c-axis disposed parallel to the substrate surface, thus configuring $H//c$ geometry in an in-plane measurement.

By considering the above hypothesis and the highly textured structure of these films, with their c-axis disposed preferentially perpendicular to the substrate surface [17], an anisotropic magnetic behaviour would then be expected by performing in-plane and out-of-plane measurements. However, this is not the case: both in-plane and out-of-plane M *vs* H measurements at 2 K (not shown) return the same shape as observed in Fig. 2(a) for $x = 0.08$ sample. Thus, we consider that, for our samples, the M_2 contribution is more likely correlated to an AFM response (discussed below) than to an anisotropic Mn^{3+} behaviour.

Non-saturated M *vs* H curves at $T \sim 2$ K are commonly observed on polycrystalline GaMnN films with high Mn^{2+} concentrations [8,9]. This behaviour is generally attributed to AFM interactions among these ions. In fact, some studies [8,9] have also described this magnetization behaviour by a single Brillouin function applied to Mn^{2+} characteristics ($J = 5/2$) and an effective temperature $T^{eff} = T + T^0$, with $T^0 > 0$. The use of $T^{eff} > T$ in the Brillouin function considers that the alignment of AFM interacting Mn spins with external field has an additional barrier (k_BT^0) beyond the real temperature effect (k_BT) [8,9]. This lowers the total magnetization in a similar way to that expected when increasing the measure temperature up to T^{eff} in an ideal paramagnetic case. Thus, higher T^0

values commonly indicate stronger antiferromagnetism and/or higher fraction of antiferromagnetic coupled Mn ions [8,9].

In our case, the optimized T^0 values were ~8 K for $x = 0.08$ sample and ~14 K for $x = 0.18$ sample. The increase on T^0 from $x = 0.08$ to 0.18 would then agree with an increase of the strength of the AFM contribution once: (i) the number of Mn^{2+} is probably increased and (ii) the mean $Mn^{2+} - Mn^{2+}$ distance is probably decreased when increasing the total Mn content (x), thus increasing the AFM coupling strength. In fact, by analysing Fig. 2(a) and (c) it is possible to note that the intensity of M_2 contribution is absolutely and relatively higher (in comparison to the others contribution) for $x = 0.18$ than for $x = 0.08$. All of the above correlations thus indicate that our M_2 contribution is probably associated with the antiferromagnetic coupling between Mn ions. These are most probably Mn^{2+} ions, which, accordingly to previous observations [8,9] and theoretical predictions [12,19], are more likely to configure AFM coupling than Mn^{3+} ions.

Discussion of the presence of a weak *M vs H* hysteresis loop at $T = 2$ K for $x = 0.18$ sample must emphasize the finding that no similar magnetic response was observed for our GaN pure film, which presented only diamagnetic behaviour. Thus, one plausible possibility is that a weak ferromagnetic phase is established among selected Mn ions giving rise to that mentioned hysteresis feature. For $T > 5$ K however, the hysteresis is not observed anymore but the contribution from the possibly still interacting Mn ions could be the reason behind the need for a high magnetic moment contribution (here approximated by M_3) to describe our *M vs H* data for $T < 50$ K. The need for M_3 contribution is emphasized in Fig. 2(d) where the paramagnetic contribution (M_1) turns to a quasi-linear curve at $T = 10$ K in contrast with the experimental data which show a smooth "S" shape for $H < 20$ kOe. Everything happens as the strength of the FM interaction, and/or the number of FM interacting Mn ions, and/or the region occupied by the interacting Mn ions are too small to lead to a robust hysteresis but they still contribute to the overall magnetization as like as the presence isolated high magnetic moment domains. An important point is that the optimized J_3 values (J_3 ~15 for $x = 0.08$ and J_3 ~20 for $x = 0.18$) obtained in this Brillouin approach cannot be taken as quantitative values, meaning that the mean number of Mn^{3+} composing each high magnetic moment domain can radically differ from that simply estimated by $J_3/J_{Mn^{3+}}$ ratio.

At this point, one could state that the isolated domains with high magnetic moment define superparamagnetism. However, no clear superparamagnetic behaviour was noticed from our temperature-dependent magnetization curves. Only paramagnetic Curie–Weiss-like curves were observed for both samples using applied fields from 0.1 to 10 kOe, as shown in Fig. 3 for 10 kOe. This could be an indication that the high magnetic moment domains are duly confined in a very small spatial region. Thus, the origin of this high magnetic moment domain could be suggested to correlate with the presence of nanometric Mn aggregates. However, no evidence for the formation of these types of aggregates or any other secondary phase was detected by XRD, HRTEM (resolution of 0.5 nm), or EFTEM (resolution of 5 nm) experiments [17]. Therefore, the most probable explanation is that a short ranged or weak FM interaction is taking place among nearest, but still diluted, Mn ions, giving rise to a localized ferromagnetic region enclosing, probably, several tens of weakly aligned Mn ions. Discussion of the FM interaction among Mn ions in GaN should emphasize that FM coupling is commonly attributed to interacting Mn^{3+} ions [12,19]. In this depiction, the short-ranged FM interaction could probably be driven via double exchange mechanisms, which would hardly lead to a robust or long ranged ferromagnetic ordering in a nanocrystalline sample.

5. Conclusions

The magnetic properties of $Ga_{1-x}Mn_xN$ nanocrystalline films with $x = 0.08$ and $x = 0.18$ were successfully characterized by field- and temperature-dependent SQUID magnetometry. Further than the dominant paramagnetic-like behaviour, particular features, as the absence of saturation at low temperatures and the presence of weak hysteresis loop, indicated the presence of secondary magnetic phases. A simple and qualitative analysis based on the Brillouin function assisted the interpretation of these secondary magnetic contributions, which were tentatively attributed to antiferromagnetic and ferromagnetic phases.

Establishing the origin of each possible magnetic interaction is beyond the scope of this work. However, the presence of multiple magnetic phases might be correlated to the nanocrystalline nature of the studied films. In this type of material, the variety of chemical and structural environment offered to the Mn sites is supposed to compose different backgrounds to the magnetic interaction mechanisms, allowing the interacting Mn to assume different magnetic states.

Acknowledgements

We would like to acknowledge the FAPESP agency (grants 2005/02249-0, 2004/12120-1 and 2006/05627-8) for funding this project, Prof. Wilson Aires Ortiz for the use of the SQUID equipment, and Prof. Alberta Bonanni and Dr. Thibaut Devillers for the fruitful discussions.

References

[1] T. Dietl, H. Ohno, F. Matsukura, Phys. Rev. B 63 (2001) 195205.
[2] T. Dietl, H. Ohno, F. Matsukura, J. Cibert, D. Ferrand, Science 287 (2000) 1019.
[3] H. Ohno, Science 281 (1998) 951.
[4] G.T. Thaler, M.E. Overberg, B. Gila, R. Frazier, C.R. Abernathy, S.J. Pearton, J.S. Lee, S.Y. Lee, Y.D. Park, Z.G. Khim, J. Kim, F. Ren, Appl. Phys. Lett. 80 (2002) 3964.
[5] S. Sonoda, S. Shimizu, T. Sasaki, Y. Yamamoto, H. Hori, J. Cryst. Growth 237–239 (2002) 1358.
[6] W. Stefanowicz, D. Sztenkiel, B. Faina, A. Grois, M. Rovezzi, T. Devillers, F. d'Acapito, A. Navarro-Quezada, T. Li, R. Jakiela, M. Sawicki, T. Dietl, A. Bonanni, Phys. Rev. B 81 (2010) 235210.
[7] X.Q. Xiu, R. Zhang, B.B. Li, Z.L. Xie, L. Chen, B. Liu, P. Han, S.L. Gu, Y. Shi, Y.D. Zheng, J. Cryst. Growth 292 (2006) 212.
[8] S. Granville, B.J. Ruck, F. Budde, H.J. Trodahl, G.V.M. Williams, Phys. Rev. B 81 (2010) 184425.
[9] M. Zajac, J. Gosk, M. Kaminska, A. Twardowski, T. Szyszko, S. Podsiadlo, Appl. Phys. Lett. 79 (2001) 2432.
[10] D. Chen, Z. Ding, S. Yao, W. Hua, K. Wang, T.X. Chen, Nucl. Instrum. Methods B 266 (2008) 2797.
[11] H. Katayama-Yoshida, K. Sato, T. Fukushima, M. Toyoda, H. Kizaki, V.A. Dinh, P.H. Dederichs, J. Magn. Magn. Mater. 310 (2007) 2070.
[12] P. Kacman, Semicond. Sci. Technol. 16 (2001) R25.
[13] J.H.D. da Silva, D.M.G. Leite, A. Tabata, A.A. Cavalheiro, J. Appl. Phys. 102 (2007) 063526.
[14] J.H.D. da Silva, D.M.G. Leite, A.R. Zanatta, J. Phys. Condens. Matter 20 (2008) 252201.
[15] D.M.G. Leite, J.H.D. da Silva, J. Phys. Condens. Matter 20 (2008) 055001.
[16] D.M.G. Leite, L.F. da Silva, A.L.J. Pereira, J.H.D. da Silva, J. Cryst. Growth 294 (2006) 309.
[17] D.M.G. Leite, T. Li, T. Devillers, Z.S. Schiaber, P.N. Lisboa-Filho, A. Bonanni, J.H. Dias da Silva, J. Cryst. Growth 327 (2011) 209.
[18] M.A. Garcia, E.F. Pinel, J. de la Venta, A. Quesada, V. Bouzas, J.F. Fernandez, J.J. Romero, M.S. Martin-Gonzalez, J.L. Costa-Kramer, J. Appl. Phys. 105 (2009) 13925.
[19] G.M. Dalpian, S.H. Wei, J. Appl. Phys. 98 (2005) 083905.